Black Sea Journal of Engineering and Science

EFFECT OF RIB SHAPE ON FLOW REGIME AND HEAT TRANSFER

Seyhun DURMUŞ[1]*

[1]*Edremit School of Civil Aviation, Balikesir University, 10145, Balikesir, Turkey*

Abstract: In current study, flow behavior and heat transfer properties in a square channel roughened with square, right triangle, isosceles triangle and circular ribs were examined. The validation test was performed for an experimental square rib case with a pitch ratio (P/e) of 9 and a blockage ratio (e/H) of 0.1. Only to examine the rib shape factor; height, base width, and rib spacing were taken the same in all cases. The study investigated the effect of various rib shapes on flow characteristics, overall thermal performances, normalized heat transfer distributions, and friction factors (pressure losses) at Reynolds numbers of 30,000 and 60,000. As a result of the numerical study, it was found that the rib shape effect did not cause as big differences in the flow properties as the blockage ratio (rib height) and pitch ratio (rib spacing) effect. In terms of the average Nusselt number enhancement, the right triangular ribbed case performed best, circular ribbed case performed worst, while the isosceles ribbed case performed better than square ribbed case. The isosceles ribbed case and right triangular ribbed case cause higher friction factor and pressure loss, while minimum friction is obtained in circular ribbed case and then in square ribbed case. As a result, in terms of overall thermal performances, right triangular ribbed case provided the best performance, followed by isosceles triangular ribbed case. The circular ribbed case produced less friction than the square ribbed case. The thermal performance of the square ribbed case was slightly higher than that of circular ribbed case.

Keywords: Rib shape, Rib-roughened channels, Convective heat transfer, Cooling ducts, CFD

1. Introduction

Turbulators are ribs in cooling channels that increase heat transfer by periodically interrupting the main flow and boundary layer. Rib-roughened ducts have many applications: Heat exchangers, solar air heaters, the electronics cooling systems, scram-jet inlets, internal cooling turbine blades, nuclear reactors, etc. There are many factors affect the aerothermal behavior of rib roughened ducts: Channel geometry (rectangular, square, trapezoidal, triangular), rib profile shape, blockage ratio, rib pitch, rib angle to the mainstream (30, 45, 60), rib configurations (staggered, transverse, V shape), 180° turn effect for multi-passed channels etc. There are many studies on these effects in the literature. Many studies have been done on channel aspect ratios (AR) in rectangular cooling ducts. The pressure drops in wide channels (AR=2:1 AR=4:1) are greater than in narrow channels (AR=1:4, AR=1:2). As a result of these studies, it was concluded that ribs increase heat transfer but cause pressure drop due to surface friction and rib form drag effect (El Hadrami et al., 2002; Lee et al., 2003; Su et al., 2004). A numerical study was carried out on the heat transfer and friction factor in a hemispherical rib roughened equilateral triangular duct (Kumar and Kumar, 2017). Many experimental studies have been conducted on trapezoidal two-pass channels (Moon et al.,

2002; Lee, 2007). The effect of rib shape, rib spacing, rib angle, rib alignment was mostly studied in square channels (Han, 2013). It has been found that a large pressure drop occurs in the U-turn zone of multi-pass channels. (Chyu, 1989). The rib height is an important factor in determining the behavior of cooling air. The blockage ratio (e/H) is typically taken in the range of 0.05-0.2 as the high blockage ratios cause an increase in friction factor and a decrease in thermal performance. The rib spacing or rib pitch to height ratio (P/e) has a significant effect on air recirculation and reattachment behavior. Rib pitch/ rib height ratios studied in the literature are typically in the 6-12 range (Keshmiri et al., 2002; Liu et al., 2006).

The rib angle-the angle of the rib to the mainstream- is another factor affecting the heat transfer coefficient. Initial studies were done on orthogonal (90°) ribs, but later studies were mostly done with transverse ribs (30°, 45°, 60°). It has been found that transverse rib arrays provide better thermal performance than orthogonal rib arrays (Han, 2007). Rib alignment configurations also affect heat transfer and flow properties. There are many studies on rib alignment configurations in the literature: staggered, discrete, parallel, truncated, continuous, V-shaped, W-shaped, etc. (Cho et al., 2000; Liu et al., 2006). The entrance length, entrance shape, refrigerant type,

numbers of ribbed walls, Reynolds number, and Prandtl number are other factors affecting the thermal performance of cooling ducts. Sharp-edge rib profiles have higher heat transfer enhancement than round rib profiles, but round ribs provide a lower friction factor that is, they cause less pressure loss. In a three-dimensional experimental study for delta-shaped and wedge-shaped rib profiles; it was concluded that delta-shaped ribs provide better thermal performance than wedge ribs (Han et al., 1993). The effect of triangular, square, and hemispherical rib shapes on heat transfer coefficients has been studied for a constant friction factor (Chandra et al., 1998). Ahn (2001) conducted a similar study of Chandra et al. (1998) and suggested that triangular ribs provide higher thermal performance. Tapered ribs with reduced in the direction of flow were found to provide higher thermal performance than square ribs (Wang and Sudden, 2007). Ekiciler (2021) studied heat and flow characteristics with the RNG k-epsilon turbulence model in a triangular rib roughened channel, using four different fluids under turbulent forced convection conditions. There are few studies on aero-thermal effects of rib shapes, in the literature because old production techniques limited the production of some rib shapes. On the other hand, the newly developed 3D metal printing technology allows the production of different rib shapes. In current study, ANSYS Fluent 19.0, a commercial computational fluid dynamics software, was used in numerical analysis to investigate the the effect of flow regime occurring in different rib shapes on heat transfer enhancement. The validation tests were performed considering the experimental case of Rau et al. (1998). The paper aims to investigate whether the rib shape is as effective as blockage ratio (rib height) and pitch ratio (rib spacing) on the flow properties. Compared with the current literature (Han, 2013), the result of the study showed that the rib shape effect did not cause as large differences in flow characteristics, as the blockage ratio and pitch ratio effect. The present study differs from the existing studies in revealing the effect of various rib shapes (square, right triangle, isosceles triangle and circular ribs) on flow characteristics, overall thermal performances, normalized heat transfer distributions, and pressure losses. In addition, all the effects examined were made for Reynolds numbers, 30,000 and 60,000, and the effect of the Reynolds number was also discussed.

2. Material and Methods
2.1. Physical Models, Grid, Boundary Conditions, and Computational Details
Computer-aided design (CAD) models of rib roughened cooling ducts generated on basis of the Rau et al. (1998)'s experimental case with a 1.5 scale. The dimensionless parameters (blockage ratio is e/Dh=0.1, the rib pitch is the P/e=9) are the same as Rau et al's experimental case. In all cases, rib heights (e) and rib base widths (w) are

taken as 15 mm and the channel height-hydraulic diameter-150 mm. To focus on the shape effect, the rib pitch and the blockage ratio are the same for all physical models. Figure 1 (a, b, c, d) shows the square, right triangular, isosceles triangular, and circular shape models. The Reynolds number is defined by the bulk velocity, not inlet velocity. The channel length (3.2 meters) has been kept long enough to minimize the adverse effects of the inlet length, adverse effect of the un-periodicity of ribs, and the adverse effect of backflow in the outlet region. The base area between the ribs was divided into 10 sub-zones as shown in Figure 1. (f), then the area-weighted local Nusselt number for each region was numerically obtained. Constant heat flux was applied to the base plate. The inlet temperature was fixed at 300 K. The plexiglass material was selected as a base and wall material. No-slip boundary conditions were applied on all the walls and ribs. Specific heat capacity and thermal conductivity of air with temperature variation were calculated by the piecewise linear functions. Coarse (node numbers~500X500), medium (node numbers~700X700), and fine (node numbers~900X900) mesh sizes were applied to the CAD models. Considering the average values of the normalized heat transfer, the fine grid (Figure 1-e) gave more consistent results with a 0.1% margin of error than the other grids. Thus, over the 810,000 of node numbers were applied to all physical models. The wall was kept near to unity, so the near-wall mesh consideration-y+ the first cell next to a wall was kept under 1.
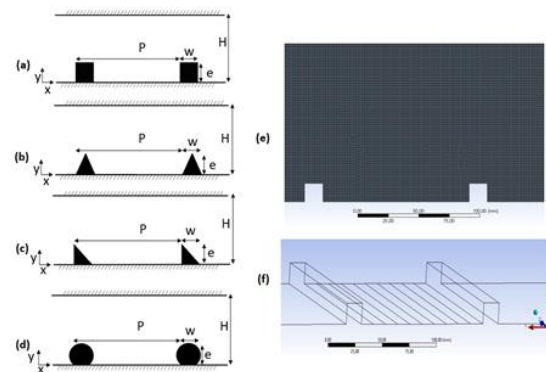

Figure 1. Square rib case (a), right triangular rib case (b), isosceles triangular rib case (c), and circular rib case (d). The generated mesh is indicated in (e) and the base area divisions are given in (f) for the local area-weighted average Nusselt number measurement.

Second-order scheme is chosen for momentum, turbulent dissipation, turbulent kinetic energy solutions. Validation tests have been performed repeatedly to find the successful turbulence models in flow pattern prediction with the experimental case. Reynolds Stress Model (RSM) produced better results than the first order Eddy Viscosity Models (EVM) models i.e. k- ε models, k-ω models. The superiority of RSM is due to fact that Reynolds stress equations contain terms of production

and body force that can respond to the effects of streamline curvature, rotation, and buoyancy (Sleiti and Kapat, 2004). Figure 2 shows heat transfer enhancement ($Nu/Nu0$) in the direction of normalized flow which includes experimental data and numerical results for some turbulence models. Reynolds Stress Model (RSM) is more successful in predicting heat transfer enhancement compared to Eddy Viscosity Models (k- ε models, SST k-ω models). In numerical simulations, the heat transfer estimates near the rib do not agree with the experimental data, while in the middle regions, the estimates are more consistent with the experimental data. Again, Keshmiri et al. (2002), in the validation of the experimental case of Rau et al. with the V2f turbulence model, they obtained a normalized heat transfer enhancement similar to the results obtained in present study.
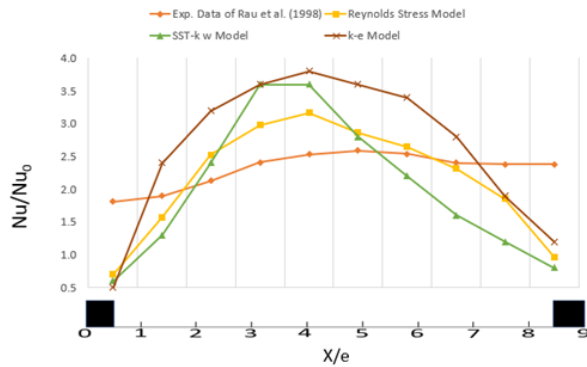

Figure 2. Numerical validation tests for square rib case including different turbulence models. The curves show the normalized heat transfer enhancement at floor.

2.2. Governing Equations and Thermohydraulic Properties

Continuity equation, conservation momentum, and energy are governing equations in computational fluid dynamics. Continuity, momentum in the x-direction, and energy equations are given equations 1, 2 and 3:

$$\frac{D\rho}{Dt} + \rho \nabla \cdot \vec{V} = 0 \tag{1}$$

$$\rho \frac{Du}{Dt} = \rho g_x + \frac{\partial \sigma_{xx}}{\partial x} + \frac{\partial \tau_{yx}}{\partial y} + \frac{\partial \tau_{zx}}{\partial z} \tag{2}$$

$$\rho c_v \frac{DT}{Dt} = \nabla \cdot k\nabla T - p\nabla \cdot \vec{V} + \mu \Phi \tag{3}$$

Local Nusselt number (Nu) is given in equations 4 and 5. The ratio of convective heat transfer to conductive heat transfer normal to the boundary. Heat transfer coefficient (h) is defined as the ratio of the heat flux and the temperature difference between the wall and the bulk air. Equation 6 explains the relationship between the shear stress and convective-conductive heat transfer ratio.

$$Nu = hD_h/k \tag{4}$$

$$h = q/ (T_w-T_b) \tag{5}$$

$$Nu = \frac{qD_h}{k(Tw-Tb)} \tag{6}$$

The normalized Nusselt number (Nu_0) is calculated from the smooth passage. The Dittus-Boelter correlation is given in the equation 7, where the Prandtl number (Pr) is 0.71.

$$Nu_0 = 0{,}023\ Re^{0,8}\ Pr^{0,4} \tag{7}$$

The friction factor (f) is the ratio of the wall shear to the dynamic pressure of the flow (equation 8). The average effective friction factor depends on pressure drop (Δp), inlet velocity, hydraulic diameter, and length scale.

$$f = \frac{\tau_w}{0.5\rho U_0^2} = \frac{\Delta P D_h}{2\rho U_0^2 L} \tag{8}$$

The normalized friction factor for a smooth passage is calculated by the Blasius equation and is simply a function of the Reynolds number (equation 9).

$$f_0 = 0.0791\ Re^{-0.25} \tag{9}$$

The pressure coefficient (equation 10) is the ratio of difference between the static pressure and the reference pressure to the dynamic pressure of the bulk air. The reference pressure was measured in the mid-section plane of any two ribs.

$$C_p = \frac{P_s - P_{ref}}{0.5\rho U_0^2} \tag{10}$$

The overall thermal performance (TEP) of the rib roughened duct is obtained from the ratio of normalized ratio of heat transfer and normalized ratio of friction factor to the power of -1/3 (equation 11).

$$TEP = \left(\frac{Nu}{Nu_0}\right)\Big/\left(\frac{f}{f_0}\right)^{-1/3} \tag{11}$$

3. Results and Discussion

In current study, the numerical simulations were performed on the ducts roughened with square ribs, isosceles triangular ribs, right triangular ribs, and circular ribs. The results of the analysis showed that the velocity distributions did not change much for the different rib shapes. Since the streamwise velocity is more dominant than the wall-normal velocity, the behavior of the streamwise velocity component is almost parallel to the resulting velocity magnitude. The wall-normal velocity initially remained unchanged, then dropped slightly to a negative value and eventually rose to a positive peak. The wall-normal velocity became a negative value along with the recirculation bubble due to flow separation. After reattachment, the wall normal velocity began to increase and reached a positive peak upstream of the rib, where the turbulent eddy propagation was maximized. In square and circular rib cases, the wall adjacent temperature became maximum

just behind the rib, especially in the bottom region, because there was a small-scale additional recirculation zone there that prevented convective heat transfer. This is also the answer why square and circular ribs perform poorly; given the increase in average Nusselt number. In front of the rib, a small-scale temperature rise occurred adjacent to the wall in the region where a new boundary layer is formed. This is the starting point of the recirculation bubble developed by the entrained flow. Since changes in temperature are much more dominant than changes in pressure, air density shows a tendency similar to change in temperature. The flow separation pattern after ribs and reattachment before the following rib are almost similar; however, the size of the bubble in the recirculation zone is greatest for the isosceles triangular ribbed case. The size of the bubble in the recirculation zone is small for the square and circular ribbed cases. The position of the reattachment point after the recirculation zone indicates the peak values of the heat transfer. The flow was reattached at 0.4 x/P for the right triangle ribbed case and at 0.5 x/P for the isosceles triangle ribbed case. Figure 3 shows the ratio of the local Nusselt number to the normalized Nusselt number between any two ribs in the Reynolds numbers 30,000 and 60,000. While the wall temperatures showed similar trends at 30,000 Reynolds numbers, the wall temperatures showed different trends at 60,000 Reynolds numbers.
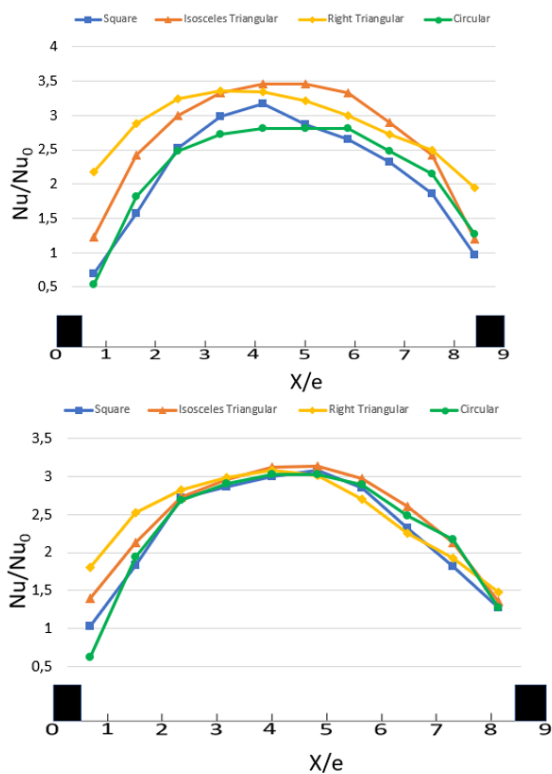

Figure 3. Normalized heat transfer-the the area-weighted average local Nusselt number of ribbed case/averaged Nusselt number of smooth duct case-distributions between any two ribs at 30,000 Reynolds numbers (up) 60,000 Reynolds numbers (down). Averaged Nusselt numbers are taken from the plane in mid-section of the duct (z=0.075 m) and from the floor.

In the 60,000 Reynolds number behind the rib region, the wall temperatures differ and then they show a similar tendency. Figure 4 shows the vector plots and Figure 5 shows the streamlines of flow velocity distributions.
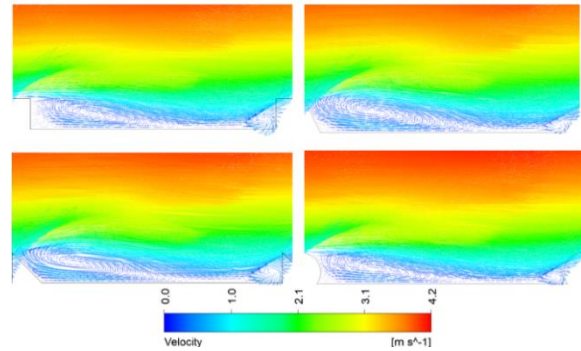

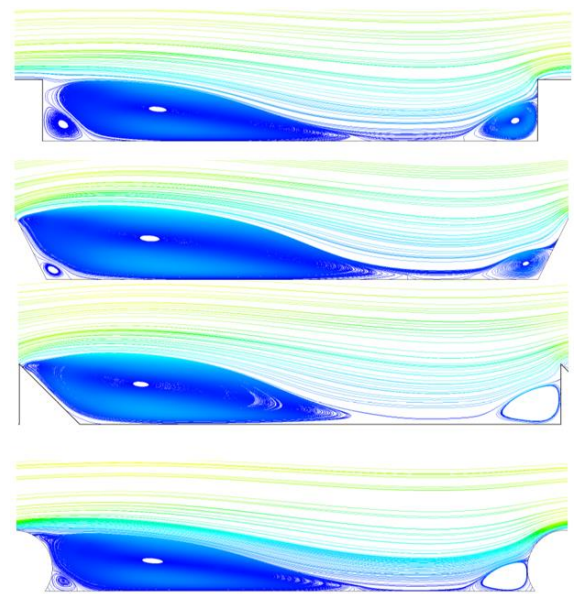**Figure 4.** Vector plots of the flow velocity distributions.

Figure 5. Illustration of streamlines for various rib shapes.

Interestingly, the inclined edges with decreasing in height in the direction of flow (right triangular and isosceles triangular) resulted in a higher normalized Nusselt number increase. If an additional performance comparison is made for the right triangular and isosceles triangular, it will be seen that the right triangular ribbed case provides better normalized Nusselt number, since the hypotenuse of the right triangular ribbed case is more inclined than the isosceles triangular ribbed case. An additional recirculation bubble was not formed behind at the base of the right triangle ribbed case. Besides, the second circulation bubble has formed in front of the rib is larger for steep obstacles. Therefore, the size of the second recirculation bubble ahead of the next ribs shows a similar tendency in the square and right triangular ribbed cases. Behind the rib (on left side of Figure 5) inclined edges generated large recirculation bubbles and steep edges generated small recirculation

bubbles. In contrast, in front of the next rib (on right side of Figure 5), steep edges generated large recirculation bubbles, while inclined edges generated small recirculation bubbles.

Fig. 6 shows the turbulence kinetic energy contours of the isosceles triangular rib and circular ribs. Turbulent kinetic energy increased between any two ribs at the height of the rib, reaching a peak around the rear corner upstream of the rib. A high turbulence kinetic energy core was formed along the line $Y/e=1$. The magnitude of turbulence kinetic energy gradually decreased towards to next rib. Also, sharp corners led to higher turbulence kinetic energy than round corners. The highest velocity magnitude occurred in the recirculation zone, followed by recovery zones. Favorable velocity gradients are their greatest value at the beginning of the reattachment zone (positive peak). Higher maximum positive velocities occurred due to the large clearance between the downstream rib and the reattachment point.
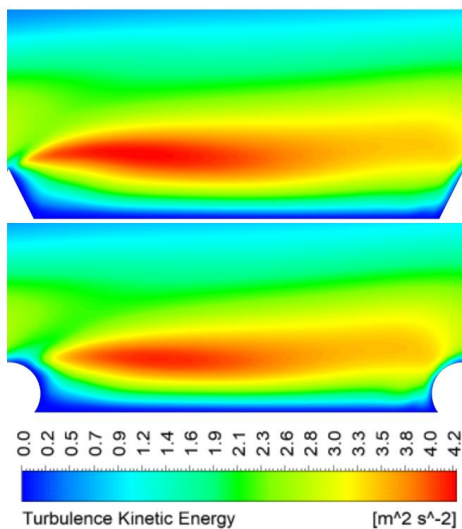

Figure 6. Turbulence kinetic energy contours of isosceles triangular ribs and circular ribs.

Figure 7 shows the normalized streamwise velocity distribution at $Y/e=0.1$ in the 30,000 and 60,000 Reynolds numbers, respectively. The right triangular ribbed case showed an unusual tendency; i.e. it tends to be isosceles triangular ribbed case in the first half (0-0.45x/P) and a square ribbed case in the second half (0.45x/P-0.9 x/P). In the 60,000 Reynolds number, the circular ribs showed a higher normalized velocity in the flow direction. Behind the ribs, the vertical motion around the recirculation zone replaced the cold mainstream against the ribbed wall. This effect resulted in a decrease in the local bulk temperature and an increase in the normalized Nusselt number ratio. For both triangular ribbed cases, the lateral dimensions of the recirculation bubble and the x/P distance of the recirculation bubble core were smaller than the square and circular ribbed cases. The extension of the recirculation bubble at the downstream of the rib

(negative peak) is similar to that of the square and circular ribbed cases. The mainstream above the ribs forced the stream in a new boundary layer through the shear layer to cope with the sudden increase in pressure. In the recirculation section, both triangular ribs show similar tendency, while differences have formed in the recovery zone. The right triangular and square ribbed cases showed a similar tendency in the recovery zone as their edge slope was similar.
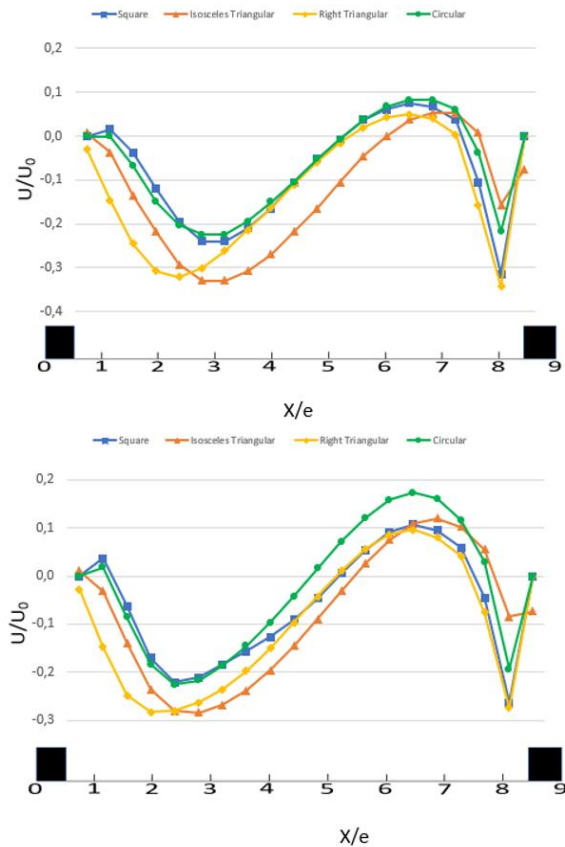

Figure 7. The distribution of the normalized streamwise velocity at $Y/e=0.1$ is in the number of 30,000 Reynolds (which is on the up side) in the number of 60,000 Reynolds (which is on the down side).

In Figure 8, the wall-normal velocity distribution (V/U0), at $Y/e=1$ is shown at 30,000 and 60,000 Reynolds numbers. Right triangular and square ribs have a high-velocity magnitude to cross steep edges. In the isosceles triangular ribbed case, the flow is more fluent, so the wall-normal velocity magnitude is lower than the others. Furthermore, the maximum streamwise velocity shifted toward the smooth sidewalls. At the top of the rib, a low-pressure zone has formed, causing a deflection in secondary flow. Unlike the 30,000 Reynolds number; the wall-normal velocities in the recovery zone have different sizes and tend to differ in the Reynolds number of 60,000.

Figure 9 shows the pressure coefficient distributions between any two ribs on the floor. In a smooth channel, the pressure drop is only a function of the wall shear stress and depends only on the skin friction drag.
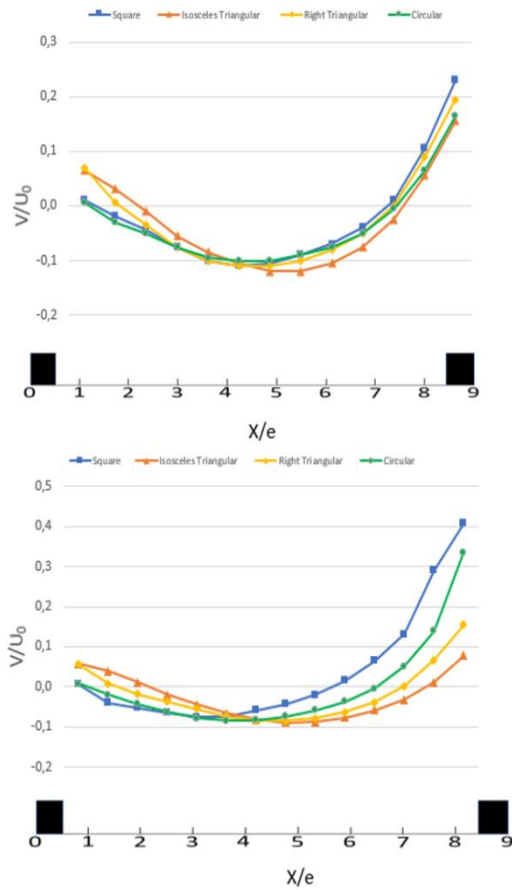
Figure 8. Wall-normal velocity distribution-V/U0 at Y/e=1 is in the number of 30,000 Reynolds (which is on the up side) in the number of 60,000 Reynolds (which is on the down side).

Jet impingement in front of the rib generated a formation of a high dynamic pressure zone. Static pressure drops abruptly due to rib form drag. Pressure coefficients around the recirculation zone are therefore negative. Pressure began to rise in the reattachment zone and reached its maximum value upstream of the rib. Due to adverse velocity gradients, the pressure behind the ribs is decreasing. The flow begins to accelerate from the reattachment zone up to the top of the ribbed wall, resulting in total pressure losses. The total pressure drop for a rib roughened channel is related to mean skin friction drag and rib form drag. The skin friction factor depends on Reynolds number and the form drag is affected by the static pressure gap between upstream/downstream regions of the ribs. Upstream of the rib, a high-pressure zone is formed due to flow impingement, while a low-pressure zone is formed downstream of the rib.

A lower pressure penalty is important for cooling channels, because it is thus possible to increase the mass flow rate of the cooling air at the same pumping power. The minimum pressure loss occurred in the square and circular ribbed case. The maximum pressure loss occurred first in right triangular rib and then in the isosceles triangular rib. Isosceles and right triangular

ribbed cases produced a higher friction factor (higher-pressure loss), while circular ribbed cases provided a minimum friction factor.
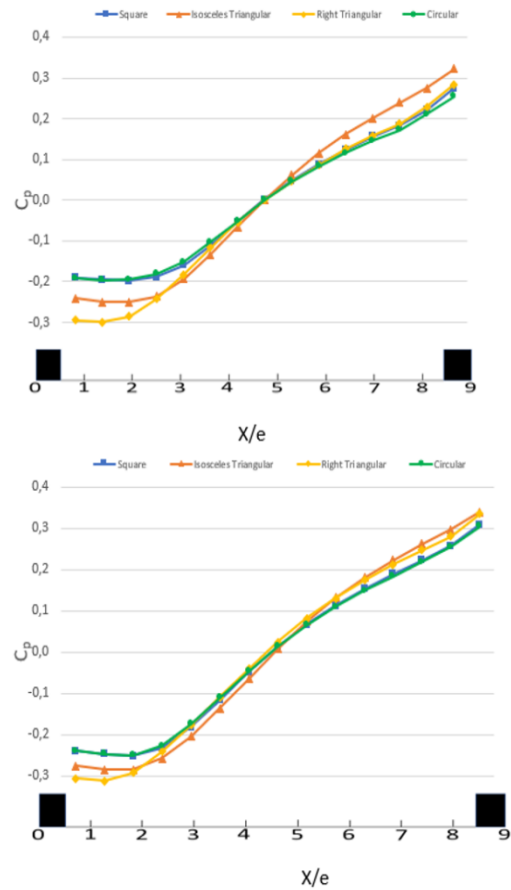

Figure 9. The pressure coefficient distributions between any two ribs is in the number of 30,000 Reynolds (which is on the up side) in the number of 60,000 Reynolds (which is on the down side).

Equation 11 gives an idea of the overall thermal efficiency by considering the heat transfer and friction factor together. Figure 10 shows the friction factor, the normalized Nusselt number, and the overall thermal performance results at 30,000 and 60,000 Reynolds numbers, respectively.

Right triangular rib form is the best rib forms for thermal performance followed by triangular rib form. The circular rib form produced least friction followed by square rib form. The thermal performance of the square ribbed case was slightly higher than circular ribbed case due to higher heat transfer enhancement. Right triangular ribbed case created the maximum friction factor, while performing the best case in terms of overall thermal performance (TEP). Unlike 30,000 Reynolds number, the effect of friction factors increased at the 60,000 Reynolds number, and the effect of the shape factor on heat transfer and overall thermal performance decreased.
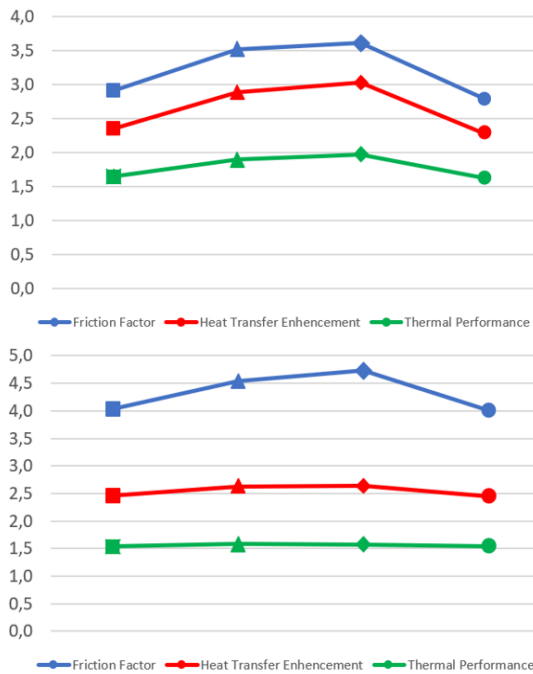
Figure 10. Representation of the friction factor averaged Nusselt numbers and overall thermal performances in the number of 30,000 Reynolds (on the up side) in the number of 60,000 Reynolds (on the down side).

4. Conclusion

In present study, detailed aerodynamical effect and heat transfer efficiency for different rib shapes in a square channel were investigated at 30,000 and 60,000 Reynolds numbers. The flow pattern at recirculation and reattachment zones have shown similar properties for all cases where P/e was 9 and e/H was 0.1. This means that the rib shape factor is not as efficient to flow properties as the influence of the blockage ratio and pitch ratio. Although a close flow characteristic occurred in different rib shapes, significant differences occurred in normalized Nusselt number, friction factors and thermal performances. The location of the reattachment point between the ribs gives an idea of the peak values of the heat transfer enhancement. The flow is reattached first in the right triangular ribbed case and then in the isosceles triangular ribbed case, so the right triangular ribbed case is the best-performing case in terms of averaged Nusselt number. Although the flow is smoother in circular ribbed case which creates less friction factor; the circular ribbed case gave the worst results in terms of averaged Nusselt number.

Behind the rib, the recirculation bubble size is larger in inclined obstacles, and in front of the rib, the recirculation bubble size is larger in upright obstacles. The ribbed shape with height decreasing in the flow direction (right triangular and isosceles triangular) showed a higher thermal performance. Since the hypotenuse of the right triangular rib form is more inclined than the isosceles triangular rib form; the right triangular ribbed case provides better thermal

performance than the isosceles triangular ribbed case. In terms of overall thermal performances (TEP), the right triangular ribbed case performed well, followed by isosceles triangular ribbed case. The circular rib form produced less friction than the square rib form, but in terms of overall thermal performances, the square ribbed case had slightly higher thermal performances than the circular ribbed case. In the number of 60,000 Reynolds, rib shape factor losses its effect on heat transfer enhancement and overall TEP compared to number of 30,000 Reynolds.

Author Contributions

SD contributed to the design and implementation of the research, to the analysis of the results and to the writing of the manuscript.

Conflict of Interest

The author declared that there is no conflict of interest.

References

Ahn SW. 2001. The effect of roughness type on friction factors and heat transfer in roughened rectangular duct. Int Comm Heat Mass Transfer, 28(7): 933-942.

Al-Hadhrami LM, Griffith TS, Han JC. 2002. Heat transfer in two-pass rotating rectangular channels (AR=2) with parallel and crossed 45o V-shaped rib turbulators. AIAA 2002: 2002-0789.

Chandra PR, Fontenot ML, Han JC. 1998. Effect of rib profiles on turbulent channel flow heat transfer. AIAA J Thermoph Heat Transfer, 12(1): 116-118.

Cho HH, Wu SJ, Kwon HJ. 2000. Local heat/mass transfer measurements in a rectangular duct with discrete ribs. J Turbomachinery, 122: 579-586.

Chyu MK. 1989. Regional heat transfer and pressure drop in two-pass and three-pass flow passages with 180-degree sharp turns. In: Proceedings of ASME 1989 International Gas Turbine and Aeroengine Congress and Exposition. June 4–8, Toronto, Ontario, Canada, pp. V004T08A024-V004T08A024.

Ekiciler R. 2021. Effects of novel hybrid nanofluid (TiO 2–Cu/EG) and geometrical parameters of triangular rib mounted in a duct on heat transfer and flow characteristics. J Thermal Anal Calorimetry, 143(2): 1371-1387.

Han JC, Huang JJ, Lee CP. 1993. Augmented heat transfer in square channels with wedge-shaped and delta-shaped turbulence promoters. Enhanced Heat Transfer, 1(1): 37-52.

Han JC, Datta S, Ekkad S. 2013. Gas turbine heat transfer and cooling technology. CRC Press, Ohio, USA, 1th ed., pp. 887.

Keshmiri A, Cotton MA, Addad Y. 2002. Numerical simulations of flow and heat transfer over rib-roughened surfaces. Int J Heat and Fluid Flow, 23(6): 750-757.

Kumar R, Kumar A. 2017. Computational fluid dynamics-based study for analyzing heat transfer and friction factor in semi-circular rib-roughened equilateral triangular duct. Int J Numerical Methods for Heat & Fluid Flow, 27(4): 941-957.

Lee E, Wright LM, Han JC. 2003. Heat transfer in rotating rectangular channels (AR=4:1) with V-shaped and angled rib turbulators with and without gaps. ASME 2003: GT2003-38900.

Liu YH, Wright LM, Fu WL, Han JC. 2006. Rib spacing effect on heat transfer and pressure loss in a rotating two-pass rectangular channel (AR=1:2) with 45-degree angled ribs.

ASME, 2006: GT2006-90368.

Moon SW, Endley S, Lau SC. 2002. Local heat transfer distribution in a two-pass trapezoidal channel with a 180 turn via the transient liquid crystal technique. J Energy Heat Mass Transfer, 24: 103-121.

Rau G, Cakan M, Moeller D, Arts T. 1998. The effect of periodic ribs on the local aerodynamic and heat transfer performance of a straight cooling channel. J Turbomach, 120(2): 368-375.

Rhee DH, Lee DH, Cho HH, Moon HK. 2003. Effects of duct aspect ratios on heat/mass transfer with discrete V-shaped ribs. ASME, 2003: GT2003-38622.

Sleiti AK, Kapat JS. 2004. Comparison between EVM and RSM turbulence models in predicting flow and heat transfer in rib-roughened channels. ASME, 2004: GT531-GT542.

Su G, Chen HC, Han JC, Heidmann D. 2004. Computation of flow and heat transfer in two-pass rotating rectangular channels (AR=1:1, AR=1:2, AR=1:4) with 45-deg Angled ribs by a reynolds stress turbulence model. ASME, 2004: GT2004-53662.

Wang L, Sunden B. 2007. Experimental investigation of local heat transfer in a square duct with various-shaped ribs. Heat and Mass Transfer, 43: 759-766.